Research Article

Essam M. Elsaid, Mohamed Abd El-Aziz, Amani S. Alruwaili, and Mohamed R. Eid*

Physical aspects of radiative Carreau nanofluid flow with motile microorganisms movement under yield stress *via* oblique penetrable wedge

https://doi.org/10.1515/ntrev-2025-0146
received April 23, 2024; accepted February 12, 2025

Abstract: Oil extraction, renewable energy, and biological heat transfer are the major applications of radiative Carreau nanofluid flow in the existence of microorganisms moving around a permeable wedge. This work examines the time-dependent flowing of two-phase Carreau nanofluid containing gyrostatic motile bacteria *via* permeable oblique wedge in the existence of heat source (sink) and thermal radiation. Magnetoelectric effect and yield stress on the flow motion of Carreau nanofluid are considered, as Carreau nanofluid is most suitable for representing different types of physics problems because it can disclose the rheology of liquids with short-chain suspension molecules and fluid crystals and because of its many uses in detergents and blood mixing, biological and medical operations. Appropriate similarity conversions are used to produce equations characterizing the system in a nondimensional mathematical model, which are subsequently resolved computationally using Runge-Kutta methodology based on the shooting approach. Attendance of yield stress boosts the surface frictional force, upsurges rates of heat and mass transfers of nanofluid, and maintains the density of bacteria significantly. Magnetoelectric effect also diminishes the rates of heat and mass transfers and increases the density of microorganisms in the nanofluid, which is beneficial for its uses. Yield stress is the greatest way to increase heat transfer rates in this nanofluid for industrial cooling. Magnetoelectric action and yield stress maintain microbe density, making it valuable for medicinal and biological procedures using useful bacteria.

*** Corresponding author: Mohamed R. Eid**, Center for Scientific Research and Entrepreneurship, Northern Border University, Arar, 73213, Saudi Arabia, e-mail: m_r_eid@yahoo.com
Essam M. Elsaid: Department of Mathematics, College of Science, University of Bisha, P.O. Box 551, Bisha, 61922, Saudi Arabia
Mohamed Abd El-Aziz: Department of Mathematics, Faculty of Science, Helwan University, Helwan-Cairo, 11795, Egypt
Amani S. Alruwaili: Department of Physics, College of Science, Northern Border University, Arar, 1321, Saudi Arabia

Keywords: Carreau nanofluid, magnetoelectric effect, bioconvection, viscous dissipation, Joule heating, yield stress

Nomenclature

A	unsteadiness parameter
B	variable magnetic field
γ	Biot number
B_0	constant magnetic field
Be	Bejan number
C_p	specific heat at fixed pressure
C_{f_x}	local surface frictional factor
E	electric parameter
Ec	Eckert number
f	dimensionless stream function
K	consistency coefficient
k	thermal conductance
k_p	porosity parameter
Lb	bioconvection Lewis number
M	magnetic parameter
n	power-law exponent
Nu_x	local Nusselt quantity
Nb	Brownian motion parameter
Nt	thermophoresis parameter
Nr	buoyancy ratio number
Pr	Prandtl number
Pe	Peclet number
Rd	radiation parameter
Re_x	local Reynolds number
Rb	bioconvection Rayleigh number
Sc	Schmidt number
T	fluid temperature
T_∞	ambient temperature of the fluid
T_w	temperature at the wall
u	speed component in the x-direction
U_e	free stream
u_w	stretching sheet velocity
v	rapidity component in the y-direction

We	Weissenberg number
x	streaming axis
y	cross-streaming axis

Greek symbols

α	thermal diffusivity
$\frac{2m}{m+1}$	wedge angle stricture
β	volumetric coefficient of the thermal expansion
θ	dimensionless temperature
ρ	fluid density
Λ	mixed convection number,
η	similarity independent variable
τ	Cauchy stress tensor
τ_1	ratio of heat capacities
τ_w	wall shear stress
ψ	stream function
Ω	yield stress
δ_1	motile microorganism difference factor

Subscripts

ω	quantities at wall
∞	quantities far away from the surface

1 Introduction

Non-Newtonian fluids include a wide range of contemporary materials and manufacturing liquids, such as particle slurries (*e.g.*, China clay, coal in water, sewage sludge), multi-phase mixtures (*e.g.*, oil-water emulsions, gas-liquid dispersion, froths and foams, melted butter) medicinal products, beauty products and amenities, coatings, manufactured lubricants in particular bodily fluids (*e.g.*, blood, cartilage fluid, saliva), and foodstuffs (*e.g.*, jellies, jams, and stews, marmalades). These substances exhibit non-Newtonian flows. The viscid stresses in a non-Newtonian fluid are determined by a nonlinear connection between the rate of deformation and the power-law fluids. Schowalter [1] introduced the first formulation of the boundary layer (BoLy) flowing for a non-Newtonian fluid and provided the criteria for the presence of a similarity solution. Acrivos *et al.* [2] derived a similarity solution for the BoLy equations of a power-law fluid streaming over a flatness sheet at a zero-degree angle. The power-law prototype is often utilized to investigate the rheological behavior of non-Newtonian fluids, namely, their pseudo-plastic and dilatant characteristics. Acrivos [3] conducted the first investigation on the flowing of a non-Newtonian power-law fluid down a vertical flatness sheet, specifically focusing on the free convection BoLy. This work specifically considered cases with highly modified Prandtl numbers. Fox *et al.* [4] examined the movement of a power-law liquid across a flatness sheet that continues to shift at an identical speed and temperature. The determination of precise solutions for the formulas dominating the flowing of non-Newtonian power-law fluids is a significant challenge. The challenge stems from both the nonlinearity and the order of the controlling differential formulas.

These fluids, which experience alterations in viscosity when exposed to shear stress, are used in many industrial operations. Typically, the viscosity of a fluid changes in response to the force applied to it. Certain fluids may exhibit a nonlinear change in viscosity for orders of magnitude greater than one. However, it is crucial to consider this phenomenon in polymeric and lubricating operations. To accommodate variations in viscosity with shearing rate, a category of the Newton principle of viscidness has been established. According to Bird *et al.* [5], these compounds are classified as generalized Newtonian fluids. The power law expression is the most direct approach for describing the flow characteristics of generalized Newtonian liquids. Nevertheless, this compositional relation has constraints that prevent it from predicting the rate of deformation and viscidness accurately for both lower and higher shearing rates. It is recommended [6] to model the whole comportment of liquids at lower and higher shearing rates using the Carreau liquid model. This archetypal has a superiority over previously stated prototypes as it precisely delineates the substances used in technical and organic manufacturing procedures [7,8]. Vessel ionophoresis necessitates the generation of chemical polymerized mixtures to enhance the differentiation of the DNA and protein molecules. The Carreau liquid archetypal offers a vantage *via* other representations by precisely defining a region inside the matter wherein the viscosity's shearing rate exhibits a linear relationship. Conversely, the power law exhibits a viscidness that reaches a limited value as the shearing rate tends to zero. The Carreau liquid style has garnered significant interest from academics in contemporary years owing to its versatile applications. Bush *et al.* [9] conducted an empirical validation by quantifying the resistance faced by a spherical shape in a Carreau liquid. This fluid behavior had been previously anticipated in a theoretical study, which was built upon the research conducted by Chhabra and Uhlherr [10]. They used the

boundary element approach and discovered a high degree of concurrence among the readings. Hsu and Yeh [11] investigated the impact of the BoLy on the dragging force experienced by two identical strict spheres interacting with Carreau liquid. The study included a range of Reynolds numbers from 0.1 to 40. Uddin *et al.* [12] used a combination of numerical and empirical methods to investigate the squeezed flow caused by the movement of a solid spherical shape into a skinny layer of non-Newtonian fluid. Tshehla's [13] studied a Carreau fluid flowing downward an oblique planer with a boundless sheet using a lubrication approximation. Speed and viscidness outlines were monitored by using an asymptotic technique to analyze the impact of flow-controlling parameters. Olajuwon [14] experimented to investigate the thermic properties of the hydro-magneto Carreau fluid by passing it over an upright penetrable surface with radiative heat flowing and thermic dispersion. Griffiths [15] successfully studied the three-dimensional BoLy flowing of a modified Newtonian liquid generated by a spinning disk, covering considerable bounds of Reynolds quantities. In contrast to prior models that did not account for viscosity, it has been discovered that the Carreau fluid framework is capable of accurately characterizing the strain rates for both very low and extremely high shearing rates.

The examination of fluid dynamics and thermal exchange across an elongated surface emerging from a narrow opening has gathered meaningful attention from several scholars because of its relevance in various industry contexts. For instance, during the extrusion process of a polymer material from a mold, there are occasions when the sheet undergoes stretching. The qualities of the finished product are influenced by the cooling rate and the rates at which the surface is stretchable when it is drawn into a cooling system. Since the groundbreaking research conducted by Sakiadis [16], which examined the flowing of a viscous fluid *via* a solid plane in motion, several elements of this topic have been researched by numerous writers over the years that followed. Crane [17] examined the flow of a BoLy in an incompressible viscous fluid moving toward a linear stretchy surface. In research by Cortell [18], the focus was on examining the performance of liquid flowing with high viscosity and the transmission of heat across a sheet that stretches in a nonlinear manner. In their study, Andersson and Kumaran [19] examined the flowing of a non-Newtonian power law liquid across a nonlinear extending surface in the BoLy. In their study, Chamkha and Al-Humoud [20] investigated the phenomenon of mixed convective heat transmission and fluid flow of non-Newtonian liquids from an absorptive plate that was located inside a porous medium. In their respective studies, Hady *et al.* [21] and Kishan and Reddy [22] examined the flowing and heat transmission of a non-Newtonian power law liquid across a planer that was being stretched, taking into account the dissipating effect of viscosity. In a study managed by Mahmoud [23], the researcher examined the impact of chemically reactive processes and changing viscidness on the flowing of a non-Newtonian viscoelastic liquid across a stretched plate that is submerged in a permeable substance. The study also evaluated how these factors affect heat transmission in the BoLy.

Several technological and manufacturing techniques include the use of magnetohydrodynamic (MHD) electrically conductive fluid. Examples of such cases include flowing meters, magneto hydropower dams, nuclear reactors, stirrers, and magneto-pumps. Understanding the solar cycle and the evolution of sunspots is crucial in the field of solar physics. Alfvén [24], in 1943, pioneered the development of MHD. MHD applications include medication delivery systems, cooling of liquid metal-based computers, and crystallization processes. The magnitude of magnetized generations has a substantial influence on MHD. Pavlov [25] introduced the idea of a magnetically driven, substantially conductance fluid flowing from an expanded plate. The phenomenon of fluid flow in an electrolyte solution across a flexible surface underneath the effect of a magnetized force has been extensively studied by many researchers [26–29]. Despite the increasing strength of the magnetized forces, the effect of Hall, caused by Hall currents, remains significant and cannot be disregarded. In both the Hall accelerations problem and flight magnetized force, the Hall currents play a critical role. The investigation of nanofluid flow on a spinning disk has been conducted by multiple investigators [30,31] using the Hall current method. Nevertheless, the phenomena of Hall currents in aggregation dynamics are disregarded.

Microorganisms are of great interest to academics, engineers, pharmacists, and technologists studying the movement of thick fluids. They have been used in several domains, including agronomy, industry, and scientific research, hence facilitating progress in these disciplines. In addition, bacteria particles have many applications in commerce and industry, including the manufacturing of bio-fuels, bio-diesel, bio-fertilizers, ethanol, and bio-microsystems. Bioconvective flowing is the occurrence of intricate patterns in fluids containing microbes. Hydrodynamic instabilities arise due to the upward movement of bacteria in response to outside influences, including gravity, oxygen concentricity variations, metabolic impetuses, and illumination fountains, accompanied by gravitation and shearing pressures. Bioconvection research has substantial implications in several scientific fields, including enzyme-based

biosensors, biofuel technology, and biological science. Khan *et al.* [32] investigated the influence of Navier slippage and magnetized field on mass and heat transfer in a nanoliquid that includes microbes. The study results indicated that strengthening the electro-magnetized force inside the magnetized field resulted in an expansion of the thickener of the border zone inhabited by moving microbes. Chakraborty *et al.* [33] conducted an analytical investigation to assess the combined influence of the magnetized field and bioconvective process on a nanoliquid. Their findings demonstrated that increasing the Eckert amount led to improved rapidity outlines. This indicates that an increased Eckert amount enhances the flowing speeds inside the nanoliquid structure. These findings specify a valuable understanding of the interaction of the magnetized force, bioconvective fluxing, and fluid-changing aspects, which might have significant consequences for the use of nanofluids. Waqas *et al.* [34] explored a bioconvective liquid including gyrotactic bacteria and nanomolecules. Their findings demonstrated that increasing the thermophoretic factor led to enhanced heat transfer. Thus, by changing the thermophoretic factor, one may improve the thermal transference properties of the bioconvective liquid, which includes both gyrotactic bacteria and nanomaterials. Many studies have focused on studying the effect of the electromagnetic field in the presence of biological convection [35–37].

Thermal transport efficacy is greatly influenced by the plate structure from which heat is transferred to the liquid in technical and manufacturing processes. Thermal gradients induce thermal energy transference, and heat exchangers play a crucial role in facilitating this phenomenon. They are extensively employed in diverse thermic implementations, playing a crucial role in the utilization of energy resources. Optimizing heat transmission *via* heat exchangers is crucial for effectively using energy. Hussanan *et al.* [38,39] investigated the convective heat transport processes, exploring the use of several kinds of nanomolecules in varied geometries. Eid [40] specifically examined the Cattaneo and Christov heat fluxing idea and its practical usage in the context of heat transfer in nanofluids. Previous research [41–45] provide unique insights and results in the area of heat transfer and nanofluids, providing access to the most current research.

1.1 Objectives

After an extensive review of previous literature and study of all the effects that have been made in closely related published articles related to the main idea, which is two-phase Carreau Bio-nanofluids flow:

(1) Th aim of this study is to examine the thermal attributes characteristics of time-dependent 2D flowing of Carreau bio-nanoliquid *via* a fixed or movement permeable wedge.
(2) The examination considers the effects of gyrostatic motile microorganisms, radiative fluxing, and solutal slippage.
(3) An analysis is conducted on the phenomena of pseudoplastic (shear thinning) and dilatation (thickening). In addition, the characteristics of the magnetoelectric effect, yield stress, Joule heating, and viscous dissipative flowing are also examined.
(4) The structure of the partial differential equations is reduced by utilizing suitable similarity variables.
(5) The shooting approach is used inside the Runge-Kutta methodology to get the computational solving.
(6) The graphs are used to examine the physical interpretation of the intriguing parameters.

1.2 Novelty

The innovation in this examination is to explore the thermal characteristics of time-dependent nanofluidic flow through a fixed or moving permeation oblique wedge. The effect of gyrostatically moving microorganisms in the presence of radiative flow and solute slippage is also studied. The study was carried out by analyzing the phenomena of pseudoplastic (shear thinning) and dilatation (thickening) in addition to examining the properties of the electro-magneto effect, yield stress, Joule heating, and viscous dissipation.

1.3 Applications

Nanofluids containing bacteria or microorganisms have a widespread selection of treatments in biological and medical microstructures, such as enzyme biomaterials and bioengineering. This is because it enhances and combines mass transfer, which is a crucial issue in many microsystems. The present advanced approach is particularly valuable in the realm of contemporary technology. The current flow issue is advantageous for enhancing the rates of heat transference. This model discovers implementations in several domains such as nanotechnological and biotechnological process, life science, electric and motorized manufacturing, heat storing strategies, preservation of nuclear-powered

systems, and biological sectors including medicine and cancer treatments.

2 Mathematical modeling

A two-dimensional viscous Carreau nanofluid flows *via* a wedge shape driven by gyrostatic motile bacteria. Radiative fluxing and heat distributions are tackled. We deemed flow *via* the wedge through

$$U_{\mathrm{w}}(x,t)=\frac{bx^{m}}{(1-ct)},\quad \text{and}\quad U_{\mathrm{e}}(x,t)=\frac{ax^{m}}{(1-ct)}, \tag{1}$$

where $U_{\mathrm{w}}(x,\ t)>0$ is for expanding rapidity and reducing the wedge as $U_{\mathrm{w}}(x,\ t)<0$. $U_{\mathrm{e}}(x,t)$ is free streaming, and a, b, c, and m are the positive constants. Wedge angle is $\Omega_1=\frac{2m\pi}{(1+m)}$ in which $\frac{2m}{(1+m)}$ is the wedging angle constraint (Figure 1). Cauchy stress tensor τ for Carreau fluid methodology is constructed by Carreau [46–48]:

$$\tau=-pI_0+\mu B_0,\quad \mu=\mu_0(1+(\Gamma_0\tilde{\gamma})^2)^{0.5(n-1)}. \tag{2}$$

The power law index bounds $0<n<1$ describes the pseudoplastic or shear-thinning fluids and $n>1$ exhibits the dilatation or shear thickness fluids. Consequently

$$\tilde{\gamma}=\sqrt{0.5(\Omega_i\Omega_j\,\tilde{\gamma}_{ij}\,\tilde{\gamma}_{ji})}=\sqrt{0.5(\mathrm{tr}(B_0^2))}, \tag{3}$$

where p is the pressure, I_0 is the identity tensor, n is the power law factor, B_0 is the first Rivlin–Ericksen fixed value,

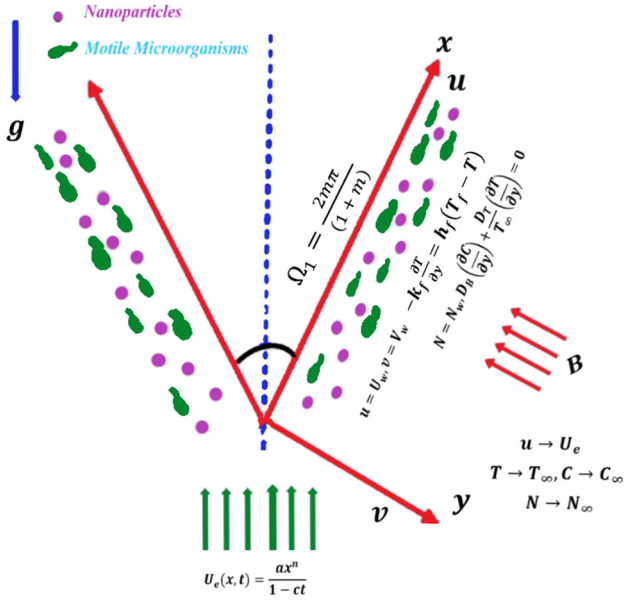

Figure 1: Flow modeling diagram.

Γ is the time material fixed amount, $\tilde{\gamma}$ is the shearing rate, and μ_0 is the zero-shearing rate. There is no association between the volume % of nanomaterials and the swimmer's orientation of the bacteria. Heat and the thickness of the gyrotactic bacteria are T_{f} and N_{w}; the surrounding temperature amount is, T_∞ and volumetric nanomolecules concentricity and motility bacteria are C_∞ and N_∞, respectively. The Carreau nanofluid framework's regulating formulas are as follows using the presumptions and BoLy approximations [46,49]:

$$\frac{\partial u}{\partial x}+\frac{\partial v}{\partial y}=0, \tag{4}$$

$$\begin{aligned}&\frac{\partial u}{\partial t}+u\frac{\partial u}{\partial x}+v\frac{\partial u}{\partial y}\\&=\frac{\partial U_{\mathrm{e}}}{\partial t}+U_{\mathrm{e}}\frac{\partial U_{\mathrm{e}}}{\partial x}+\nu_{\mathrm{f}}\frac{\partial^2 u}{\partial y^2}\left[1+\Gamma^2\left(\frac{\partial u}{\partial y}\right)^2\right]^{\frac{n-1}{2}}\\&+\nu_{\mathrm{f}}(n-1)\Gamma^2\frac{\partial^2 u}{\partial y^2}\left(\frac{\partial u}{\partial y}\right)^2\left[1+\Gamma^2\left(\frac{\partial u}{\partial y}\right)^2\right]^{\frac{n-3}{2}}\\&-\frac{\nu_{\mathrm{f}}}{K^*}[u-U_{\mathrm{e}}]+\frac{\sigma_{\mathrm{f}}B^2}{\rho_{\mathrm{f}}}\left[\frac{E_0}{B}-u+U_{\mathrm{e}}\right]\\&+\frac{1}{\rho_{\mathrm{f}}}[\rho_{\mathrm{f}}\beta g(1-C_\infty)(T-T_\infty)-g(\rho_{\mathrm{p}}-\rho_{\mathrm{f}})(C-C_\infty)\\&-g\gamma(N-N_\infty)(\rho_{\mathrm{m}}-\rho_{\mathrm{f}})]\cos\left(\frac{m\pi}{m+1}\right)-\alpha_0=0,\end{aligned} \tag{5}$$

$$\begin{aligned}&\frac{\partial T}{\partial t}+u\frac{\partial T}{\partial x}+v\frac{\partial T}{\partial y}\\&=\alpha_{\mathrm{f}}\frac{\partial^2 T}{\partial y^2}+\frac{(\rho C_{\mathrm{p}})_{\mathrm{s}}}{(\rho C_{\mathrm{p}})_{\mathrm{f}}}\left[D_{\mathrm{B}}\frac{\partial C}{\partial y}\frac{\partial T}{\partial y}+\frac{D_{\mathrm{T}}}{T_\infty}\left(\frac{\partial T}{\partial y}\right)^2\right]\\&-\frac{1}{(\rho C_{\mathrm{p}})_{\mathrm{f}}}\frac{\partial q_{\mathrm{r}}}{\partial y}-\frac{\sigma_{\mathrm{f}}B^2}{(\rho C_{\mathrm{p}})_{\mathrm{f}}}\left[u-U_{\mathrm{e}}-\frac{E_0}{B}\right]^2,\end{aligned} \tag{6}$$

$$\frac{\partial C}{\partial t}+u\frac{\partial C}{\partial x}+v\frac{\partial C}{\partial y}=D_{\mathrm{B}}\frac{\partial^2 C}{\partial y^2}+\frac{D_{\mathrm{T}}}{T_\infty}\frac{\partial^2 T}{\partial y^2}, \tag{7}$$

$$\frac{\partial N}{\partial t}+u\frac{\partial N}{\partial x}+v\frac{\partial N}{\partial y}=D_{\mathrm{m}}\frac{\partial^2 N}{\partial y^2}-\frac{\tilde{b}w_0}{C_\infty}\frac{\partial}{\partial y}\left[N\frac{\partial C}{\partial y}\right], \tag{8}$$

where u and v are in x and y orientations, respectively; volumetric absorptive nanomolecules is C; thermal diffusivity is α_{f}. $(\rho C_{\mathrm{p}})_{\mathrm{f}}$ and $(\rho C_{\mathrm{p}})_{\mathrm{s}}$ are conventional fluid heat capacitance and nanomolecules effectiveness heat capacitance. Exposed boundary backgrounds are [46–48]

$$\left.\begin{aligned}&u=U_{\mathrm{w}},\ \ v=V_{\mathrm{w}},\ \ N=N_{\mathrm{w}},\ \ D_{\mathrm{B}}\left(\frac{\partial C}{\partial y}\right)+\frac{D_{\mathrm{T}}}{T_\infty}\left(\frac{\partial T}{\partial y}\right)=0,\\&-k_{\mathrm{f}}\frac{\partial T}{\partial y}=h_{\mathrm{f}}(T_{\mathrm{f}}-T)\ \text{ at }\ y=0,\\&u\to U_{\mathrm{e}},\ \ T\to T_\infty,\ \ C\to C_\infty,\ \ N\to N_\infty\ \text{ as }\ y\to\infty.\end{aligned}\right\} \tag{9}$$

Rosseland approximation, $q_r = -\frac{4\sigma_0}{3K^*}\frac{\partial T^4}{\partial y}$ (σ_0 is Stefan–Boltzmann fixed value and K^* is the absorbing factor). T^4 may be conveyed by Taylor series. Ascending T^4 about T_∞ and avoiding relatively higher components takes $T^4 \approx 4T_\infty^3 - 3T_\infty^4$. Under such supposition, we obtain $q_r = -\frac{16\sigma_0 T_\infty^3}{3K^*}\frac{\partial T}{\partial y}$. By employing the formulas for movement and energy, we may obtain a set of ordinary differential equations (ODEs) by the specified modifications [46]

$$\eta = y\sqrt{\frac{(m+1)U_e}{2\nu_f x}},\ \psi = \sqrt{\frac{2\nu_f x U_e}{(m+1)}}f(\eta),\ U_e = \frac{ax^m}{1-ct},$$
$$\theta = \frac{T-T_\infty}{T_f - T_\infty},\ \phi = \frac{C-C_\infty}{C_\infty},\ \chi = \frac{N-N_\infty}{N_w - N_\infty}. \tag{10}$$

By incorporating certain similarity parameters, equations (5)–(8) transform into subsequent dimensional formulations.

$$\begin{aligned}[1+nW_e^2 f''^2][1+W_e^2 f''^2]^{\frac{n-3}{2}} f''' - \left(\frac{2m}{m+1}\right)[f'^2-1] \\ + ff'' - k_p[f'-1] - A\left[f' + \frac{1}{2}\eta f'' - 1\right] \\ + M[E - f' + 1] + \Lambda[\theta - \mathrm{Nr}\phi \\ - \mathrm{Rb}\chi]\cos\left(\frac{m\pi}{m+1}\right) - \Omega = 0,\end{aligned} \tag{11}$$

$$\left[1+\frac{4}{3}\mathrm{Rd}\right]\theta'' + \mathrm{Nb}\phi'\theta' + N_T\theta'^2 + \mathrm{Pr}\left[f\theta' - \frac{A}{2}\eta\theta'\right] - \mathrm{Ec}M\mathrm{Pr}[f'-E-1]^2 = 0, \tag{12}$$

$$\phi'' + \frac{\mathrm{Nt}}{\mathrm{Nb}}\theta'' + \mathrm{Sc}\left[f\phi' - \frac{A}{2}\eta\phi'\right] = 0, \tag{13}$$

$$\chi'' + L_b\left[f\chi' - \frac{A}{2}\eta\chi'\right] - \mathrm{Pe}[(\chi+\delta_1)\phi'' + \phi'\chi'] = 0, \tag{14}$$

subject to

$$\left.\begin{aligned} &f(0) = -f_w,\ f'(0) = \frac{U_w}{U_e} = \lambda,\ \theta'(0) = \gamma[\theta(0)-1], \\ &\mathrm{Nb}\phi'(0) + \mathrm{Nt}\theta'(0) = 0,\ \chi(0) = 1, \\ &f'(\infty) = 1,\ \theta(\infty) = \phi(\infty) = \chi(\infty) = 0. \end{aligned}\right\} \tag{15}$$

The dimensionless parameters are

We $= \sqrt{\frac{\Gamma^2(m+1)U_e^3}{2\nu_f x}}$ is the Weissenberg number, $k_p = \frac{2x\nu_f}{K^*(1+m)U_e}$ is the porosity number, Nb $= \frac{\tau_1 D_B}{\alpha_f}C_\infty$ is the Brownian motion parameter, Nt $= \frac{D_T}{T_\infty}\frac{\tau_1}{\alpha_f}[T_f - T_\infty]$ is the thermophoresis parameter, Lb $= \frac{\nu_f}{D_m}$ is the bioconvection Lewis number, $A = \frac{2cx}{(1+m)(1-ct)U_e}$ is the unsteadiness parameter, Pe $= \frac{\tilde{b}\,w_0}{D_m}$ is the Peclet number, Ec $= \frac{U_e^2}{(C_p)_f(T_f - T_\infty)}$ is the Eckert number, Pr $= \frac{\nu_f}{\alpha_f}$ is the Prandtl number, Rd $= \frac{4\sigma^* T_\infty^3}{k_f k^*}$ is the radiation parameter, $\delta_1 = \frac{N_\infty}{(N_w - N_\infty)}$ is the motile microorganism difference factor, $M = \frac{2x}{(1+m)U_e}\frac{\sigma_f B^2}{\rho_f}$ is the magnetic parameter, and $\gamma = \frac{h_f}{k_f}\left(\frac{2\nu_f x}{(m+1)U_e}\right)^{\frac{1}{2}}$ is Biot number.

This study focuses on surface frictional force, local Nusselt quantity, local Sherwood quantity, and thicknesses of local motility numbering of bacteria (C_{fx}, Nu_x, Sh_x, and Nh_x, respectively) as key physical factors related to momentum, thermal outlines, fractional size of absorbance, and bacterial motility movement [46,47,50].

$$C_{fx} = \frac{\tau_w}{\rho_f U_e^2}\bigg|_{y=0},\ \mathrm{Nu}_x = \frac{xq_j}{k(T_f - T_\infty)},$$
$$\mathrm{Sh}_x = \frac{xq_w}{D_B C_\infty},\ \mathrm{Nh}_x = \frac{xq_m}{D_m(N_w - N_\infty)}. \tag{16}$$

The wall-shearing stress represented by τ_w, the surface heat flowing indicated by q_j , the wall mass fluxing indicated by q_w, and the motility thickener marked by q_m are expressed as follows [45–47]:

$$\tau_w = -\mu_f\frac{\partial u}{\partial y}\left[1 + \frac{\Gamma^2}{\sqrt{2}}\left(\frac{\partial u}{\partial y}\right)^2\right]^{0.5(n-1)}\bigg|_{y=0},$$
$$q_j = \left[-k\left(\frac{\partial T}{\partial y}\right) + q_r\right]\bigg|_{y=0}\ q_w = -D_B\frac{\partial C}{\partial y}\bigg|_{y=0}, \tag{17}$$
$$q_m = -D_m\frac{\partial N}{\partial y}\bigg|_{y=0}.$$

In dimensionless outline, equation (16) gives

$$\sqrt{\frac{2}{m+1}}\sqrt{\mathrm{Re}_x}C_{f_x} = [1 + W_e^2 f''^2(0)]^{0.5(n-1)}f''(0), \tag{18}$$

$$\sqrt{\frac{2}{m+1}}\frac{\mathrm{Nu}_x}{\sqrt{\mathrm{Re}_x}} = -\left[1 + \frac{4\ \mathrm{Rd}}{3}\right]\theta'(0), \tag{19}$$

$$\sqrt{\frac{2}{m+1}}\frac{\mathrm{Sh}_x}{\sqrt{\mathrm{Re}_x}} = -\varphi'(0), \tag{20}$$

$$\sqrt{\frac{2}{m+1}}\frac{\mathrm{Nh}_x}{\sqrt{\mathrm{Re}_x}} = -\chi'(0), \tag{21}$$

where $\mathrm{Re}_x = \frac{xU_e}{\nu_f}$ is the local Reynolds quantity.

3 Computational procedure

The nonlinear ODEs (11)–(14) beside the boundary conditions (15) form a two-point boundary value problem. To resolve these formulas computationally, we have chosen the Runge Kutta Fehlberg integration method using the

shooting approach (Figure 2). Initially we transform these nonlinear formulas to first-order differential equations as described below:

$$k_1 = f,\ \ k_2 = f',\ \ k_3 = f'',\ \ k_4 = \theta,\ \ k_5 = \theta', \\ k_6 = \phi,\ \ k_7 = \phi',\ \ k_8 = \chi,\ \ k_9 = \chi'. \tag{22}$$

Utilizing these additional variables, the set of formulas (11)–(14) may be reformulated as follows:

$$k_3' = \frac{1}{[1 + nW_e^2(k_3)^2][1 + nW_e^2(k_3)^2]^{\frac{n-3}{2}}} \\ \times \left[\left(\frac{2m}{m+1}\right)(k_2^2 - 1) - k_1k_3 + k_p(k_2 - 1) \right. \\ + A(k_2 + 0.5\,\eta\, k_3 - 1) - \Lambda(k_4 - \mathrm{Nr}k_6 \\ \left. - \mathrm{Rb}k_8)\,\cos\left(\frac{m\,\pi}{m+1}\right) - \Omega - M(E_0 - k_2 + 1)\right], \tag{23}$$

$$k_5' = \left(\frac{3}{3 + 4\ \mathrm{Rd}}\right)\left[\mathrm{Pr}\left(\frac{A}{2}\eta\, k_5 - k_1k_5\right) - \mathrm{Nb}\, k_5k_7 - \mathrm{Nt}\, k_5^2 \right. \\ \left. + M\ \ \mathrm{Ec}\ \ \mathrm{Pr}\,(k_2 - E - 1)^2\right], \tag{24}$$

$$k_7' = \mathrm{PrLe}\left[\frac{A}{2}\eta\, k_7 - k_1k_7\right] - \frac{\mathrm{Nt}}{\mathrm{Nb}}k_5', \tag{25}$$

$$k_9' = \mathrm{Lb}\left[\frac{A}{2}\eta k_9 - k_1k_9\right] + \mathrm{Pe}[k_7'(k_8 + \delta_1) + k_7k_9]. \tag{26}$$

The constraints on the boundary may be expressed for the new variables as follows:

$$k_1(0) = -f_w,\ \ k_2(0) = \lambda,\ \ k_3(0) = \varepsilon_1,\ \ k_4(0) = \varepsilon_2, \\ k_5(0) = -\gamma[1 - k_4(0)],\ \ k_6(0) = \varepsilon_3, \\ k_7(0) = -\frac{\mathrm{Nt}}{\mathrm{Nb}}k_5(0),\ \ k_8(0) = 1,\ \ k_9(0) = \varepsilon_4, \tag{27}$$

where $k_3(0) = \varepsilon_1$, $k_4(0) = \varepsilon_2$, $k_6(0) = \varepsilon_3$, $k_7(0) = -\frac{\mathrm{Nt}}{\mathrm{Nb}}k_5(0)$, and $k_9(0) = \varepsilon_4$ are the unknown initial conditions. We use the shooting approach to ascertain these unidentified variables.

The alternative set of boundary conditions (15) is expressed as follows:

$$k_2(\infty) = 1,\ \ k_4(\infty) = 0,\ \ k_6(\infty) = 0,\ \ k_8(\infty) = 0. \tag{28}$$

The initial guess values ε_1, ε_2, ε_3, ε_4 and ε_4 are selected and the fifth-order Runge-Kutta-Fehlberg integration scheme with step-size $\Delta\eta = 0.001$ is applied to obtain the solutions of the system (11)–(14) satisfying the condition (28). Then, we compare the calculated values of $f'(\eta)$, $\theta(\eta)$, $\phi(\eta)$, and $\chi(\eta)$ at η_∞ with the provided boundary constraints $f'(\eta_\infty) = 0, \theta(\eta_\infty) = 0, \phi(\eta_\infty)$, and $\chi(\eta_\infty)$ and regulate the values of $f''(0)$, $\theta'(0)$, $\phi'(0)$, and $\chi'(0)$ applying "Newton-Raphson method" to give better approximations

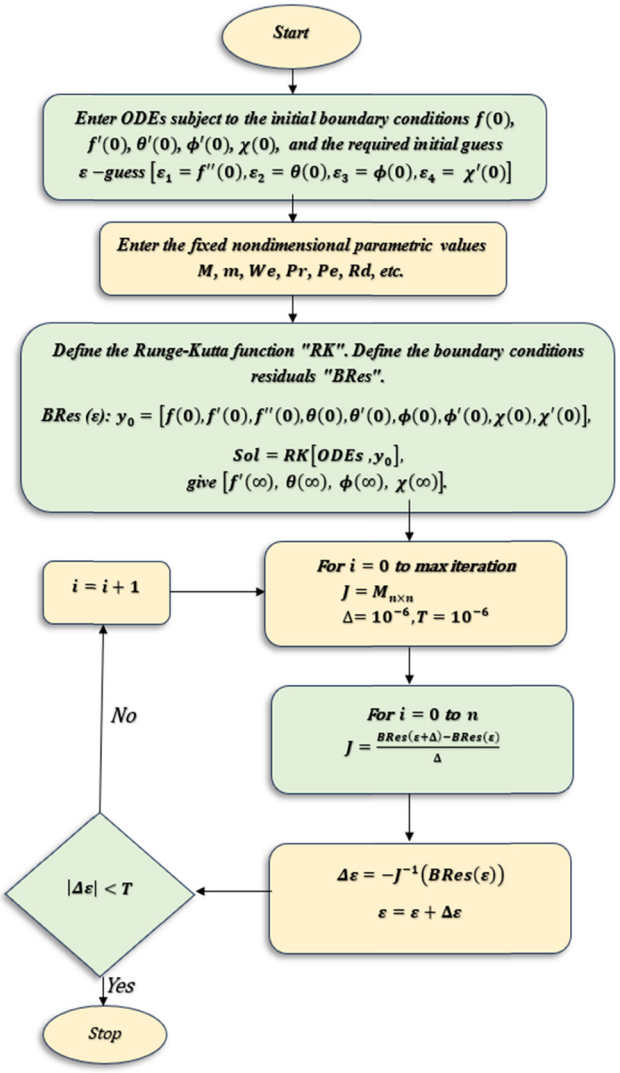

Figure 2: Numerical flow diagram.

for the required solution. The procedure is reiterated until the outcomes achieve the requisite precision of 10^{-6}, hence satisfying the convergence criteria.

4 Validation

A comparative analysis using existing data is undertaken in a constrained way to evaluate the correctness of the utilized approach. We compare our findings for the local Nusselt number for certain Prandtl number values and wedge angle parameters with the restricting examples presented by Khan *et al.* [46] and Gangadhar *et al.* [47] (Table 1). The current findings exhibit strong concordance with those in previous studies [46,47]. This gives confidence to our numerical computations.

5 Results and discussion

In this work, the mathematical modeling and computational calculations for the thermal analysis of the flowing of a two-dimensional Carreau nanofluid *via* a permeable wedge in the existence of gyrostatically moving bacteria were inspected and organized. The Carreau nanofluid was taken because it can explain the attributes of shear thinning and thickness. In addition, the magnetoelectric effect and the inclination of this wedge at an angle are considered. The flow characteristics of the nanofluid are simulated by outlines of velocity, temperature, concentration, and distributions of microorganisms. Mixed convection is used for thermal analysis of the flow field that will arise as a result of the temperature differences between the nanofluid and the surrounding environment. This research also focuses on studying the influences of the convection boundary constraints, yield stress as well as the effect of the presence of thermal radiative fluxing. During the numerical calculations process, the parameter values were taken as fixed values as follows: $M = 0.2$, $E = 0.1$, $\mathrm{Ec} = 0.2$, $\Omega = 0.05$, $f_w = -0.1$, $\mathrm{Nb} = 0.1$, $\mathrm{Nt} = 0.1$, $m = 0.1$, $\mathrm{Pr} = 6.2$, $\mathrm{Le} = 10$, $\mathrm{We} = 2$, $k_p = 0.2$, $A = 0.1$, $\Lambda = 0.4$, $\mathrm{Nr} = 0.1$, $\mathrm{Rb} = 0.1$, $\mathrm{Rd} = 0.2$, $\mathrm{Lb} = 1$, $\delta_1 = 2$, $\lambda = 0.1$, and $\mathrm{Pe} = 0.2$, with only the variable being examined changed. The examination of Carreau nanofluids in the presence of motile microorganisms with the effects of electromagnetic fields is of much importance due to the variety of different uses of this type of fluid in bioengineering, biomedicine, blood research, treatment of diseases, and others concerning human health and the prevention from infectious and epidemiological diseases.

Figure 3(a)–(d) determine the connection between the magnetized parameter M and the flowing speed $f'(\eta)$, temperature $\theta(\eta)$, concentration $\phi(\eta)$, and field of microorganisms of the nanofluid $\chi(\eta)$, respectively. It is obvious that the magnetized parameter M works to upsurge the rapidity (Figure 3(a)) and temperatures of the nanofluid (Figure 3(b)), diminish its concentration near the BoLy (Figure 3(c)), and then the opposite happens by moving away from the wedge surface. Also, the accretion magnetized parameter M leads to reduce the field of microorganisms (Figure 3(d)). It can be observed that this happens in the situation of dilatant nanofluid and Pseudoplastic nanofluid. It is remarked that the rapidity and temperature of dilatant nanofluids is lower than that of pseudoplastic nanofluids. It can also be observed that moving away from the BoLy, the concentration of dilatant nanofluids is higher than that of pseudoplastic nanofluids. The range of dilatant nanofluids is very close to that of pseudoplastic nanofluids in the case of the field of microorganisms. Physically, the cause of this is because of the fact that dilatant nanofluids are higher in dynamic viscosity than pseudoplastic nanofluids, which makes them lower in flow rapidity and higher in temperatures because they retain more thermal energy stored inside the particles that make up the nanofluid. Figure 4(a)–(c) depict the change in the rapidity $f'(\eta)$, temperatures $\theta(\eta)$, and concentration of the nanofluid $\phi(\eta)$ according to the change in the electric parameter E. It was noted that the boost in the electric parameter M raises both the rapidity (Figure 4(a)) and temperature of the nanofluid (Figure 4(b)) clearly and noticeably, but on the contrary, it reduces the concentration of the nanofluid (Figure 4(c)), and that is close to the BoLy, and then gradually moving away from it, relative stability occurs, so the concentration of the nanofluid does not change with an improvement in the electric parameter E. This is because boosting the electrical parameter has a role in stimulating the molecules that make up the fluid to move, that is, increasing the kinetic energy within

Table 1: Comparison of $(2 - \beta)^{1/2}\,\mathrm{Re}^{-1/2}\,\mathrm{Nu}_x$ for different values of Pr and β when $n = 1$ and $\gamma \to \infty$ (constant wall temperature) with $f_w = \mathrm{Nt} = \mathrm{Rd} = \mathrm{Nb} = \mathrm{Nr} = \mathrm{Rb} = \lambda = 0$

	$\beta = 0$			$\beta = 0.3$		
Pr	**Ref. [46]**	**Ref. [47]**	**Current findings**	**Ref. [46]**	**Ref. [47]**	**Current findings**
0.1	0.198129	0.1980314	0.1980.316	0.209152	0.2090754	0.2090756
0.3	0.303718	0.3037174	0.3037171	0.327829	0.3278290	0.3278289
0.6	0.391675	0.3916751	0.3916755	0.428924	0.4289244	0.4289247
0.72	0.418091	0.4180913	0.4180911	0.459551	0.4595511	0.4595506
1.0	0.469600	0.4696000	0.4696005	0.519519	0.5195184	0.5195182
2.0	0.597234	0.5972339	0.5972336	0.669045	0.6690446	0.6690444
6.0	0.867278	0.8672775	0.8672775	0.987268	0.9872675	0.9872677
10.0	1.029747	1.0297472	1.0297472	1.179130	1.1791300	1.1791300

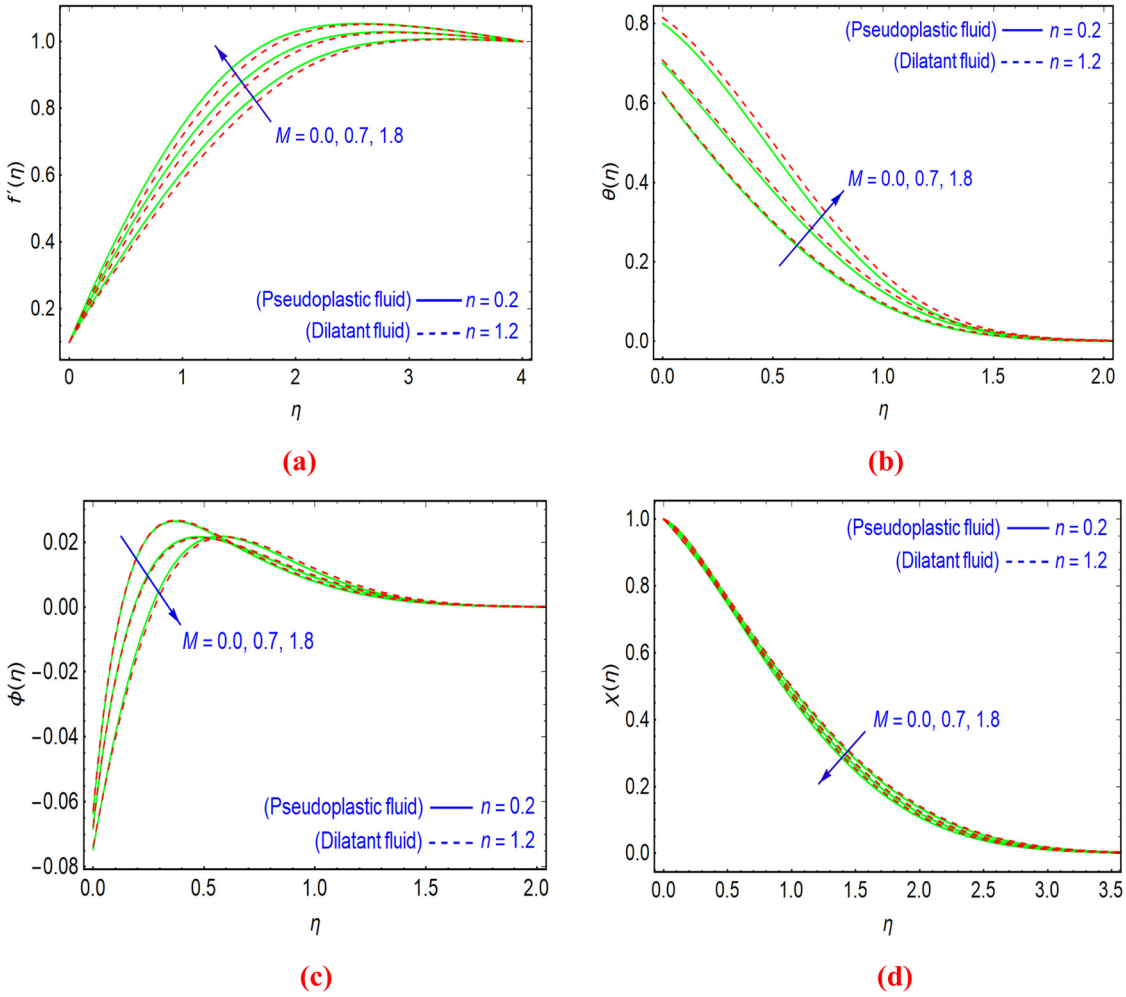

Figure 3: *M vs* (a) velocity, (b) temperature, (c) concentricity, and (d) microorganism.

them and increasing the collisions between them, which leads to an upsurge in the rate of speed and temperature of the fluid nanoparticles, thus lowering the concentration on it. As a result of their higher viscosity, dilatant nanofluids have fewer collisions and less kinetic energy than pseudoplastic nanofluids. The consequences of the electric parameter M on the field of microorganisms have not been considered due to its weak effect on this field. The reason for this is that its effect on the electric field is less than the effect of the fluid molecules that constitute the largest part of the flow process. Figure 5(a) and (b) probe the change in both temperature $\theta(\eta)$ and concentration $\phi(\eta)$ of the nanofluid as a result of the change in the Eckert number Ec. We notice clearly that a rise in the Eckert quantity raises the temperature of the nanofluid (Figure 5(a)). Moreover, it works to reduce the concentration rates of the nanofluid near the wall of the wedge, and moving away from it, the concentration begins to shrink (Figure 5(b)). Physically, the height away from the BoLy can be described because the Eckert quantity depends primarily on kinetic energy. As the Eckart number upsurges, the kinetic energy surges, and thus the temperature of the nanofluid rises as a result of collisions of its constituent molecules. The concentration near the external wall of the wedge reduces and rises away from it.

Figure 6(a)–(g) shows the effect of the mass fluxing factor f_w on each of the rapidity, temperatures, concentration, and microorganism profiles of the nanofluid. If $f_w > 0$, this expresses the injection condition, and if $f_w < 0$, this expresses the suction condition when the wedge surface is permeable. It can be remarked that in the case of suction (Figure 6(a)–(d)), that is, when $f_w < 0$, the mass fluxing parameter clearly raises the rapidity of the nanofluid, and it also lowers both the temperatures,

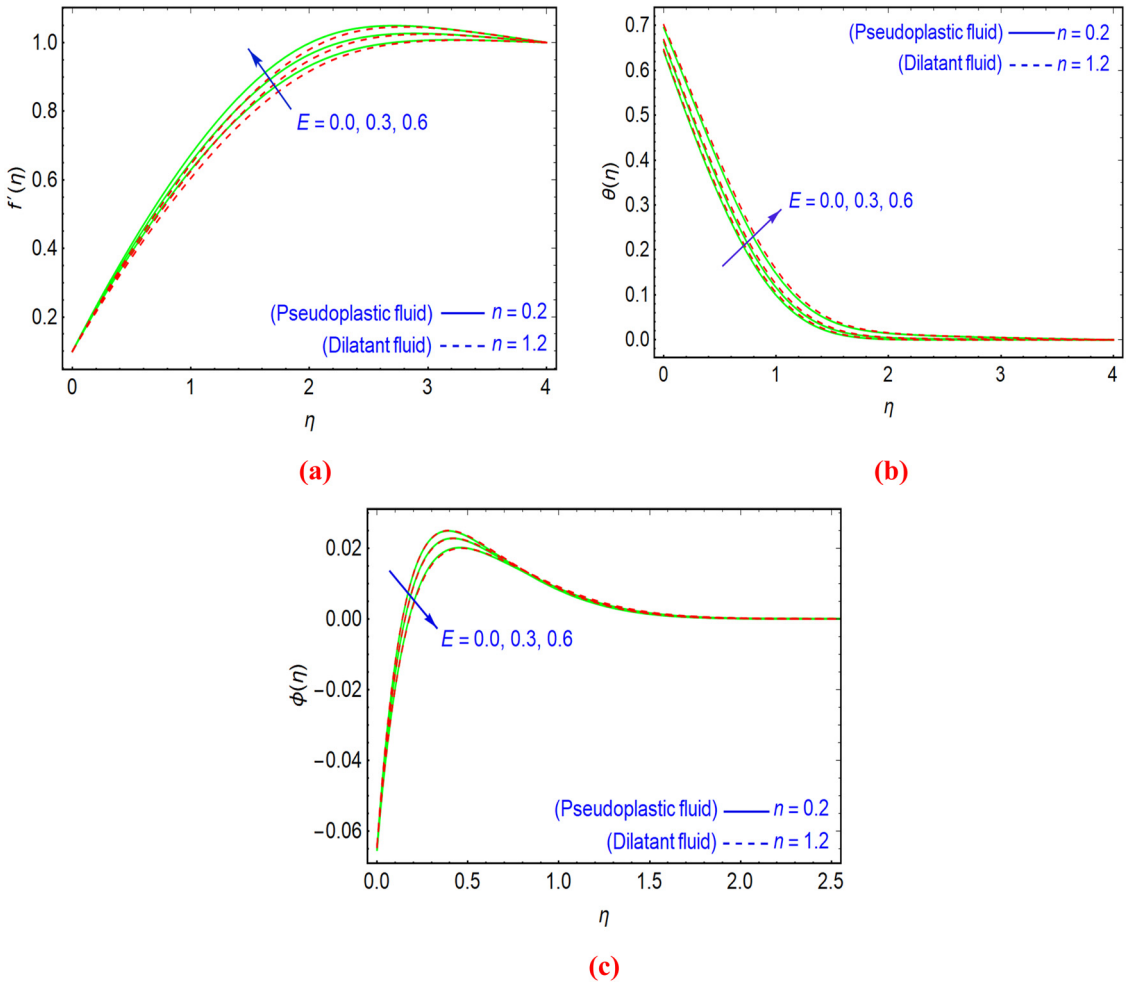

Figure 4: E *vs* (a) velocity, (b) temperature, and (c) concentricity outlines.

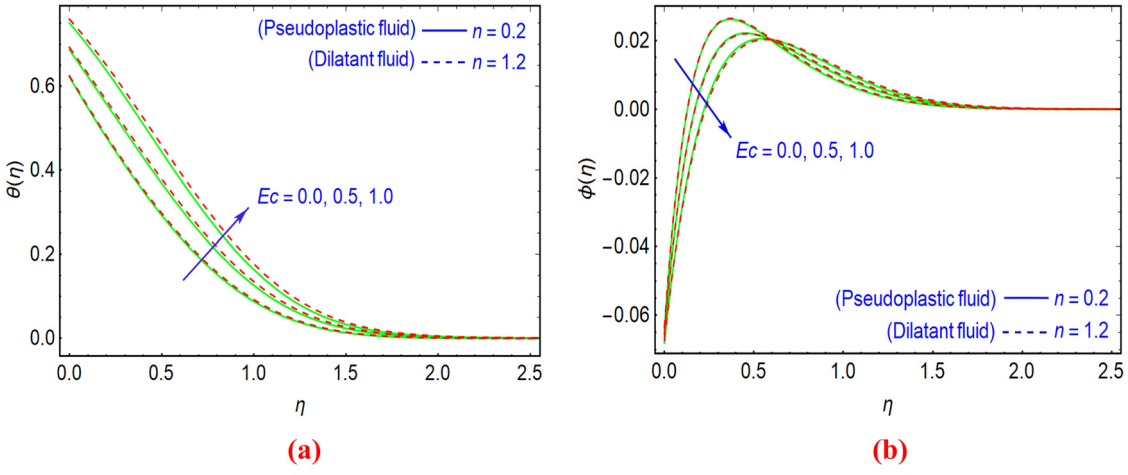

Figure 5: Ec *vs* (a) temperature and (b) concentricity outlines.

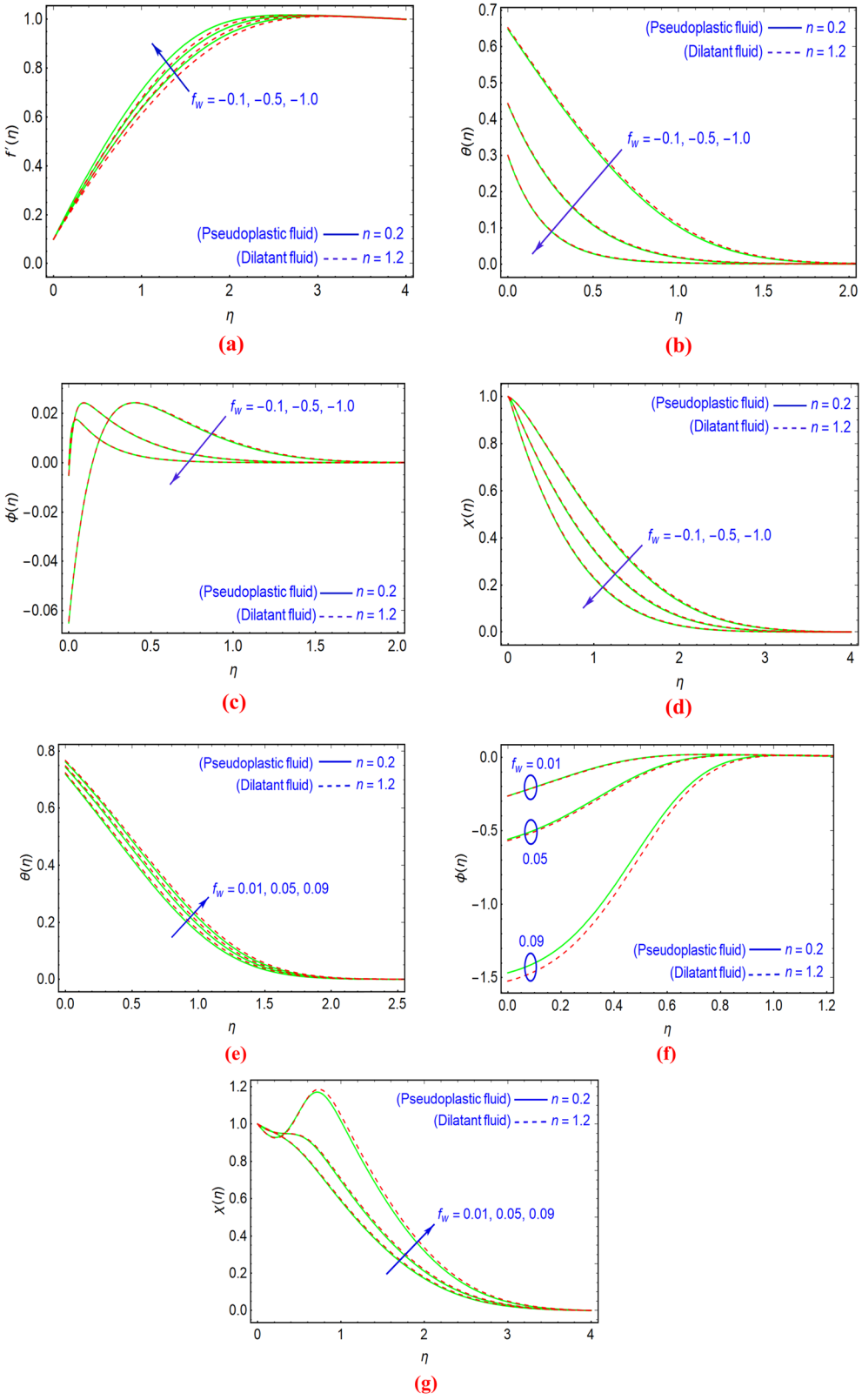

Figure 6: f_w *vs* (a) velocity, (b) and (e) temperature, (c) and (f) concentration, and (d) and (g) microorganism.

concentration, and the microorganisms' outlines. The opposite happens in the case of injection $f_w > 0$. We notice that the temperatures improve, as well as the outlines of microorganisms (Figure 6(e) and (g)). While it happens, the concentration takes its way in the opposite direction with the increase in the value of the mass fluxing factor, as shown in Figure 6(f). The mass fluxing parameter f_w is one of the parameters that has the most influence on the dynamic viscidness of the nanofluid. Therefore, the greater the mass fluxing parameter, the lower the viscidness of the fluid, and thus the effect of this on its temperatures and concentration. A higher mass fluxing value results in wider interspaces between the molecules in the nanofluid, making their interconnections smaller. Then, concentration and temperatures are weakened. In addition, the profile of microorganisms is greatly affected and thus begins to reduce as well. Figure 7(a)–(c) displays the relation between the number of Biot γ and each of the deviations occurring in the outlines of temperature $\theta(\eta)$, concentration $\phi(\eta)$, and microorganisms $\chi(\eta)$. It can be seen that the upsurge in the numbers of Biot, that is, the thermal convective at the BoLy or the convective boundary constraints, leads to a boost in the temperatures (Figure 7(a)), the concentration (Figure 7(b)), and the outline of the microorganisms of the nanofluid (Figure 7(c)). Since the ratio of the thermal resisting to conduction inside the nanofluid to the resisting to convection on the surface of the nanofluid expresses the condition of thermal convection and thus the numbers of Biot, the greater the number of Biot, the greater the ratio of thermal resistance to conduction, that is, the lower the rates of heat transference inside the nanofluid, and thus the temperature inside it upsurges as a result. It also retains the thermal energy of its constituent molecules. This thermal resistance to conduction raises the concentration and thus also raises the profile of microorganisms inside the nanofluid.

The yield stress is the stress that is applied in order to exceed the orderly flow of the nanofluid, and it is one of

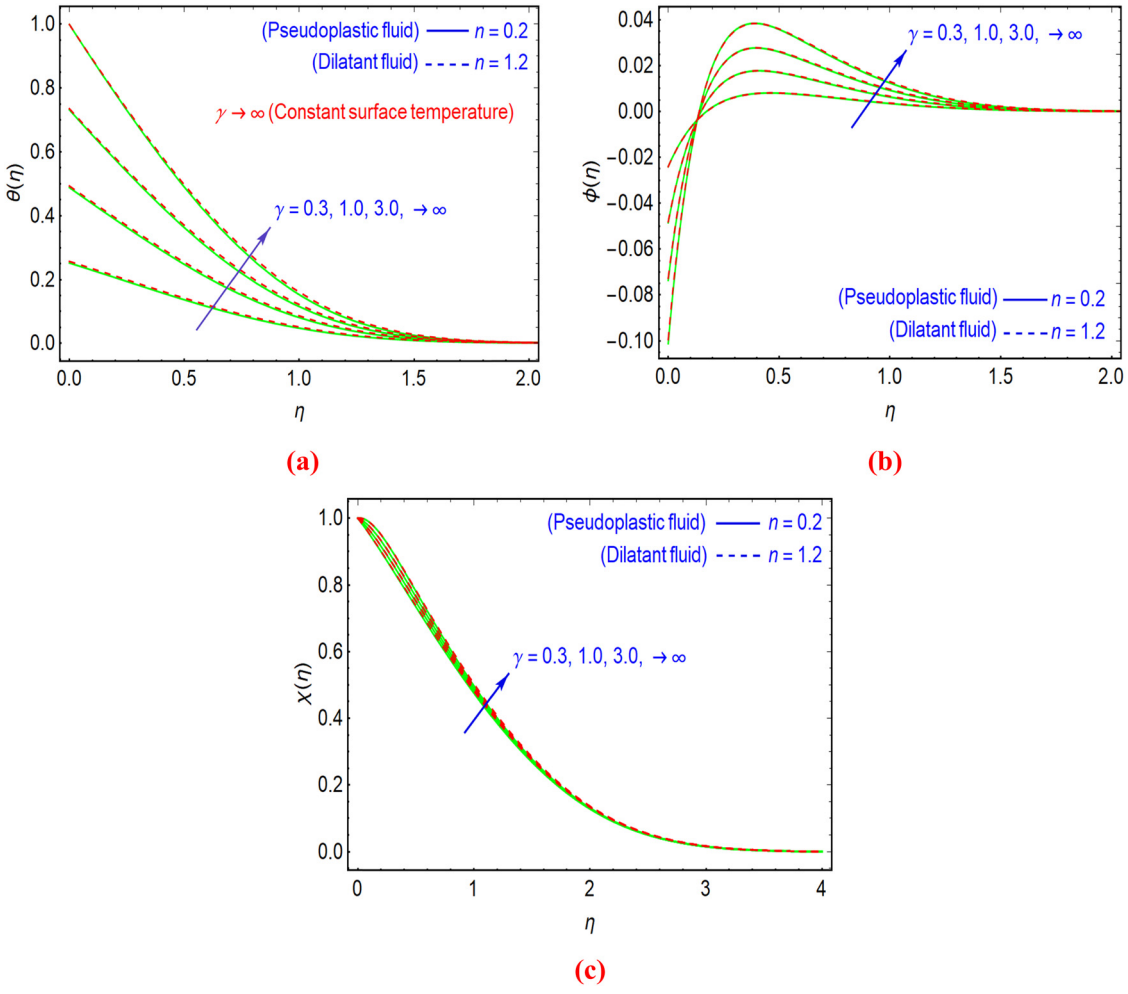

Figure 7: γ *vs* (a) temperature, (b) concentration, and (c) microorganism profiles.

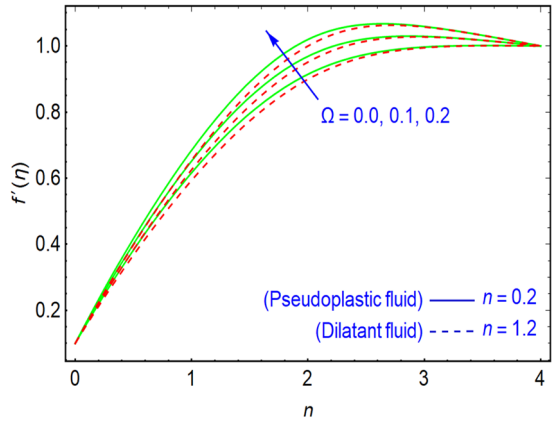

Figure 8: Ω *vs* velocity.

the important factors in many industrial processes such as coating operations, pumping, and spreading processes. Therefore, Figure 8 demonstrates the modification in flow rapidity of the nanofluid $f'(\eta)$ according to the changes in the yield stress parameter Ω. It can be viewed that the changes in the yield stress lead to a significant increment in the velocity outline away from the BoLy, which means that it improves the flowing process of the nanofluid in the case of thinning and thickening of the shear. Figure 9 illustrates the consequence of the exponent parameter m of the wedge angle and its role in the rapidity outline $f'(\eta)$ of the nanofluid. It appears that the greater the exponent parameter m, the greater the flow rapidity of the nanofluid, especially during movement outside the BoLy of the wedge in the region of the center layers of the nanofluid for both dilatant and pseudoplastic nanofluids. This illustrates whenever the worth of the exponential variable m rises according to the relationship it has with the angle of the wedge, the angle of the wedge declines, and consequently, the flowing becomes easy and smooth without any impedance of surface inclination. The concentration outline $\phi(\eta)$ begins to upsurge near the surface of the wedge, that is, next to the BoLy, and then it begins to shrink as a result of the increase in the Brownian diffusion coefficient Nb, as seen in Figure 10. The reason for this is that the Brownian movement of the molecules that make up the fluid raises the concentricity outline close to the wall and then by moving outside the wall inside the nanofluid, the frictional forces between the molecules diminish, and thus the interparticle spaces between them upsurge, which significantly reduces the nanofluid concentration. Figure 11(a)–(c) portray the effects of thermophoretic factor Nt on the temperature $\theta(\eta)$, concentration $\phi(\eta)$, and the microorganisms outlines $\chi(\eta)$. It is recorded that thermophoresis Nt raises the temperature profiles of the nanofluid and also raises the concentration outline, but inside the nanofluid, near the BoLy, it declines it. Also, thermophoresis raises the file of microorganisms. This can be explained by the fact that thermophoresis is the force of transference that occurs due to the existence of temperature differences within the nanofluid. These differences in turn lead to a increase in temperature (Figure 11(a)) and a rise of the concentration (Figure 11(b)) inside the nanofluid away from the surface, in addition to that it works to elevate the file of microorganisms (Figure 11(c)).

Figure 12(a)–(d) highlights the dependencies of the change in the convective boundary constraint (Biot number) γ on the surface frictional force, heat, and mass transfer rates, as well as the density of bacteria. It is noted that the number of Biot raises the surface frictional force for both thinning and thickening of shearing. It is also perceived that in the situation of dilatant nanofluids, the surface frictional force is much greater than it is in the case of pseudoplastic nanofluids, as shown in Figure 12(a).

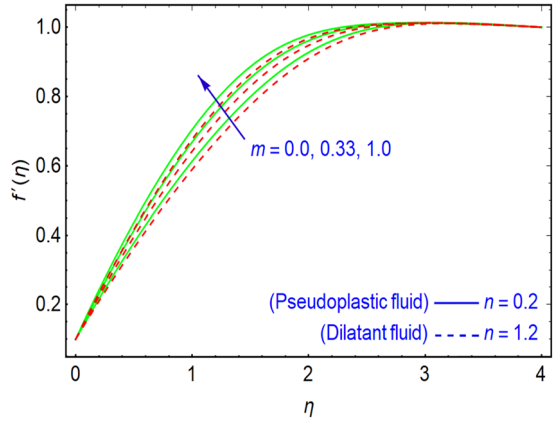

Figure 9: m *vs* velocity.

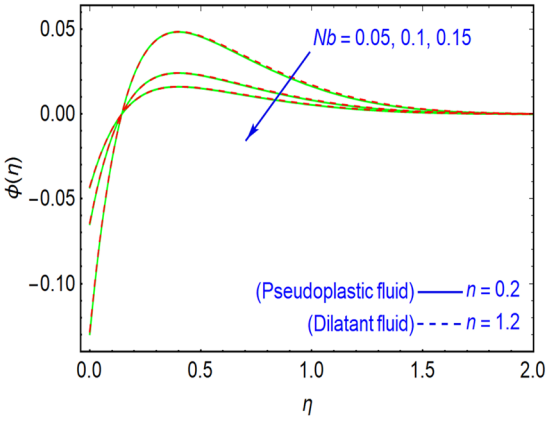

Figure 10: Nb *vs* concentration profiles.

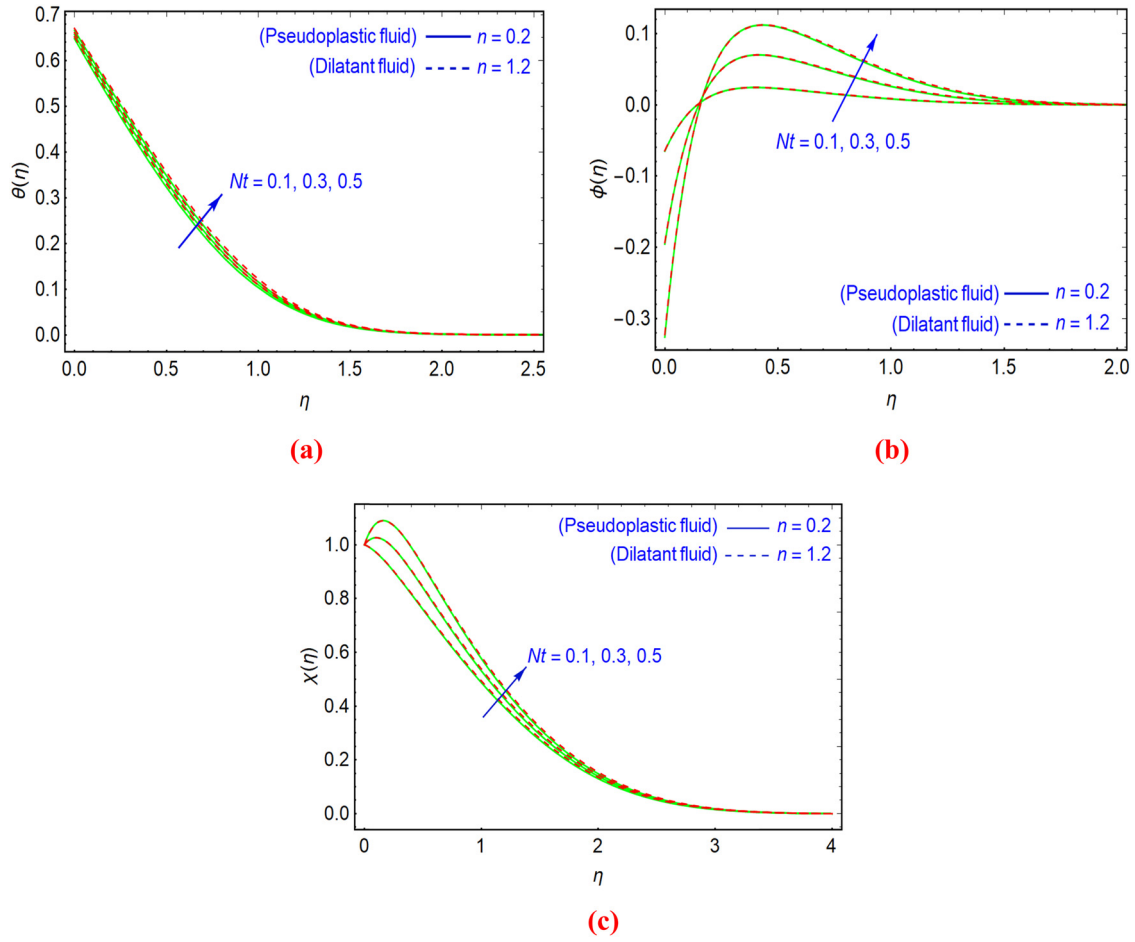

Figure 11: Nt *vs* (a) temperature, (b) concentration, and (c) microorganism profiles.

Figure 12(b) illustrates an important result, that is, Biot number γ increase the rate of heat transference for both nanofluids, but it is remarked that pseudoplastic nanofluids have higher rates of heat transference than dilatant nanofluids as a result of the change in the convection boundary constraints. The same effect occurs in the case of mass transference, which is observed in Figure 12(c). It is found that the rates of mass transfers increase with increasing Biot number γ, a steady and clear accretion, and that nanofluids of the pseudoplastic type are higher in rates of mass transfers than dilatant nanofluids. The opposite of this effect occurs in the density of microorganisms. We notice that with increasing Biot number, the density of microorganisms declines, and this is expected, as increasing the condition of convection works to reduce the microorganisms and their density inside the nanofluid clearly for both nanofluids, as snowballing convective boundary constraints works to raise the temperatures of the fluid. Noticeably it works to get rid of microorganisms and thus their density is lost significantly Figure 12(d). Figure 13(a)–(d) presents the effects of the electric parameter E on the surface frictional force, rates of heat and mass transfers, and the density of microorganisms, respectively. It is evident that surface frictional force improves with an enhancement in the electric parameter (Figure 13(a)). On the contrary, the heat transfer rates lessen with the electric parameter more clearly, as is the case in mass transfer rates (Figure 13(b) and (c)). While it is noticed that the exact opposite happens with the density of microorganisms, their density increases with the increase in the electric parameter (Figure 13(d)). This shows that the electric parameter is a major aspect in reducing the rates of heat and mass transfers keeping the fluid at its temperature and concentration as it is and preserving the microorganisms and their density. When using beneficial microorganisms inside the nanofluid, the electric parameter stimulates the increase of useful microorganisms confined to the nanofluid for use in research purposes related to blood research and the treatment of infectious and epidemic diseases.

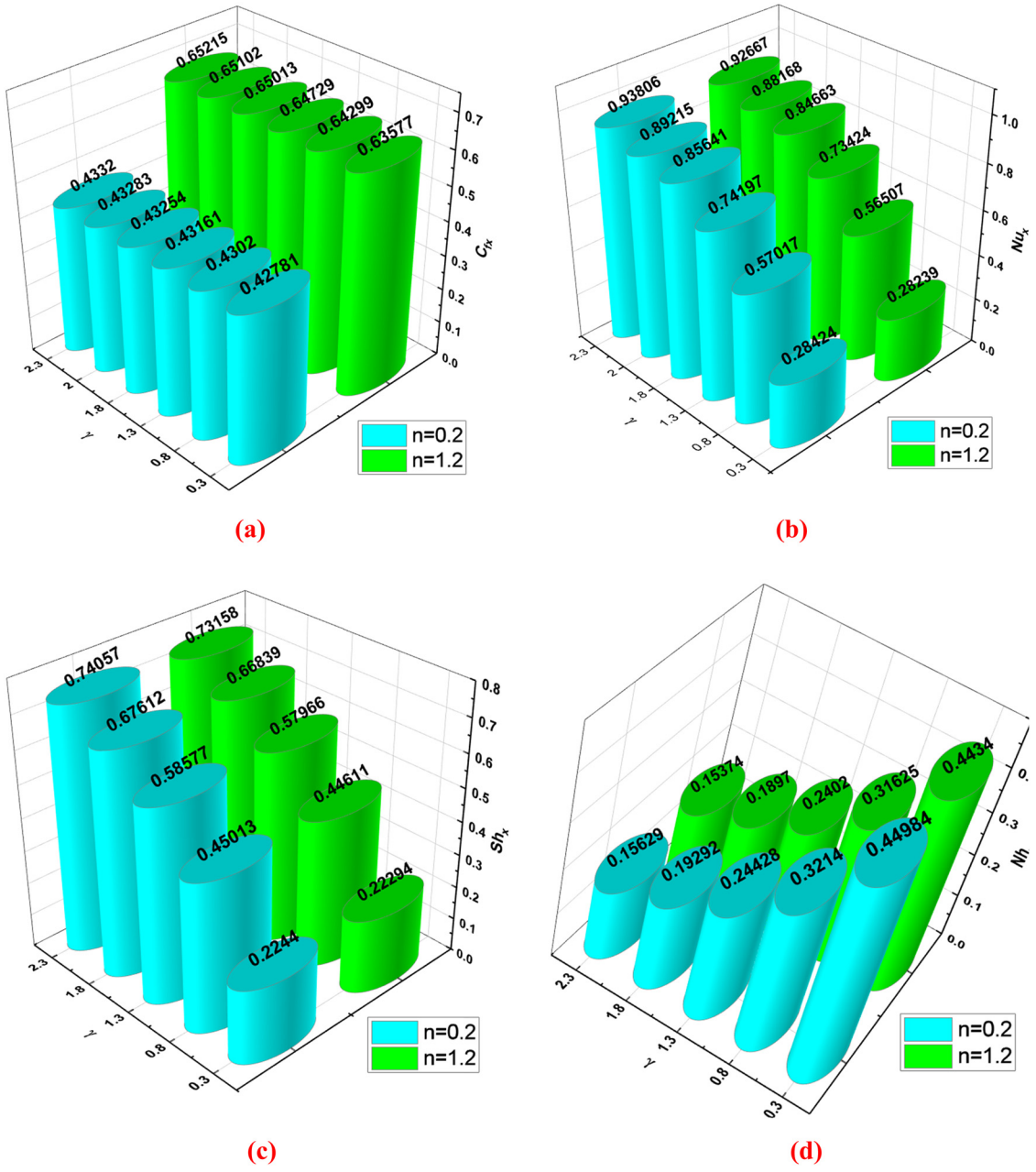

Figure 12: γ *vs* (a) frictional factor, (b) Nusselt number, (c) Sherwood number, and (d) microorganism density numbers.

Table 2 establishes the influence of the magnetized variable M, the electrical factor E, the yield stress Ω, the heat source (sink) variable f_w, the exponent factor m, and the Eckert number Ec on both the surface frictional force $C_{f_x}\,\mathrm{Re}_x^{1/2}\left(\frac{2}{m+1}\right)^{1/2}$ and the rates of heat transfer $\mathrm{Nu}_x\,\mathrm{Re}_x^{-1/2}\left(\frac{2}{m+1}\right)^{1/2}$. It can be mentioned that the surface frictional force is boosted by M, E, Ω, m, and Ec, while f_w diminishes the frictional force. The rates of heat transference are increased by Ω, f_w, and m, while M, E, and Ec decrease the rates of the transference. Snowballing the yield stress lessens the viscosity and thus enhances heat transfer while increasing the electrical parameter induces electrokinetic flow and thus works with the magnetic parameter to upsurge thermal diffusion through the effect of Lorentz forces. This shows the importance of the magnetized parameter M in maintaining the temperatures stored in the nanofluid and the use of the nanofluid in heating processes in industrial processes and smart homes. It also demonstrates the use of yield stress Ω in cooling processes for engineering and biological applications because it

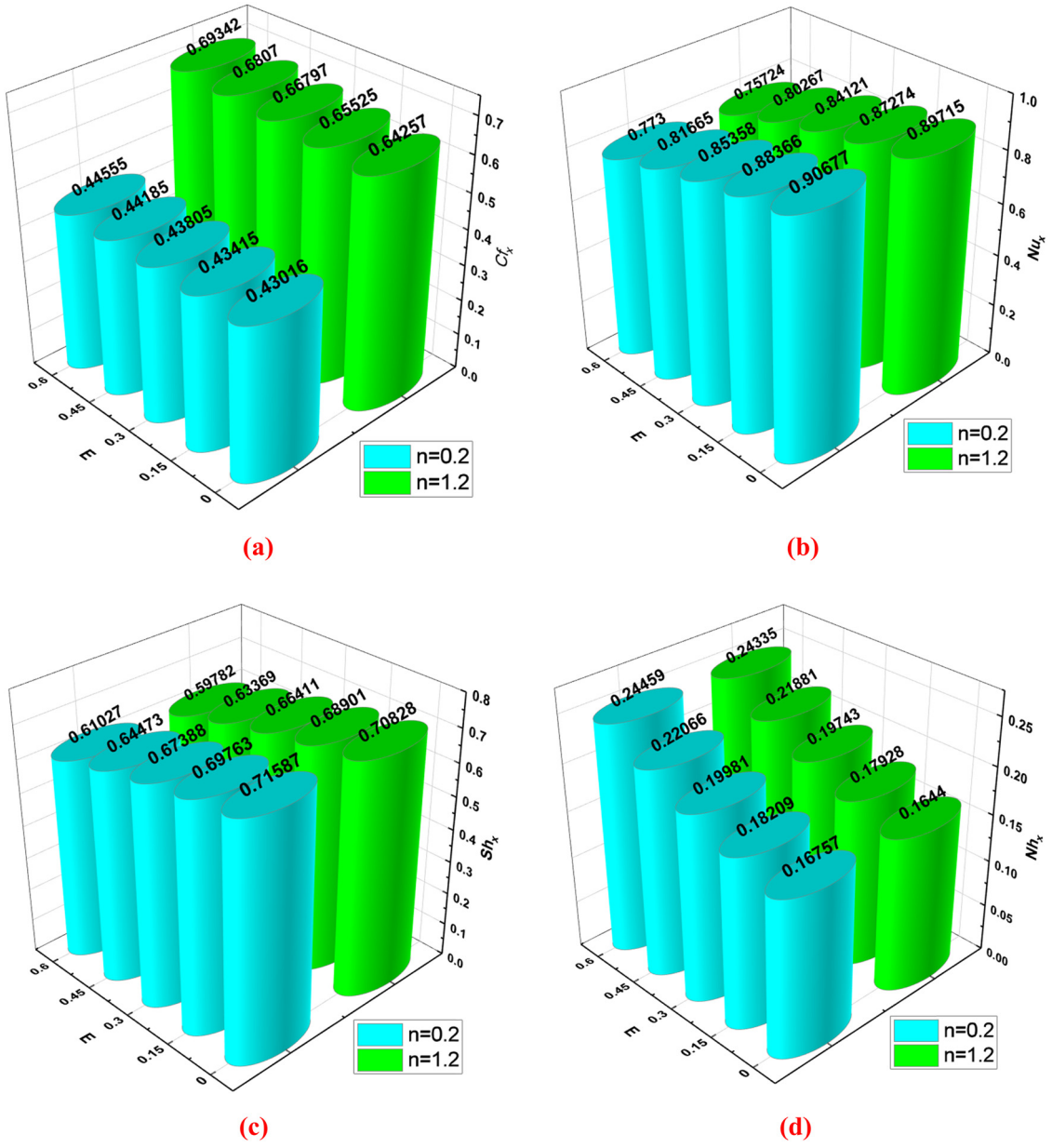

Figure 13: E *vs* (a) frictional factor, (b) Nusselt number, (c) Sherwood number, and (d) microorganism density numbers.

improves the rates of heat transference of the nanofluid. Table 3 determines the outcomes of the magnetized parameter M, the electrical parameter E, the yield stress Ω, the heat source (sink) parameter f_w, the Brownian movement Nb, and the Eckert quantity Ec on both the mass transference rates $\mathrm{Sh}_x\mathrm{Re}_x^{-1/2}\left(\frac{2}{m+1}\right)^{1/2}$ and the density of microorganisms $\mathrm{Nh}_x\mathrm{Re}_x^{-1/2}\left(\frac{2}{m+1}\right)^{1/2}$. It is clarified that all the aforementioned parameters raise the density of microorganisms inside the nanofluid, which is useful in maintaining the quantity of these microorganisms within the nanofluid if they are beneficial microorganisms and using them in various biological and medical processes. While it is remarked that the yield stress parameter is the only one that raises the rates of mass transference of the nanofluid, in complete contrast to the rest of the parameters under examination, it lowers the rates of mass transference within the nanofluid.

Table 2: Outcomes of the local wall frictional force coefficient $C_{f_x}\,\mathrm{Re}_x^{1/2}\left(\frac{2}{m+1}\right)^{1/2}$ and local Nusselt quantity $\mathrm{Nu}_x\,\mathrm{Re}_x^{-1/2}\left(\frac{2}{m+1}\right)^{1/2}$ for diverse amounts of M, E, Ω, f_w, m, and Ec with Pr = 6.2, Le = 10, Lb = 1, We = δ_1 = 2, k_p = Rd = Pe = 0.2, A = Nr = Nt = Rb = λ = 0.1, and Λ = 0.4

M	E	Ω	f_w	m	Ec	$C_{f_x}\mathrm{Re}_x^{1/2}\left(\frac{2}{m+1}\right)^{1/2}$		$\mathrm{Nu}_x\mathrm{Re}_x^{-1/2}\left(\frac{2}{m+1}\right)^{1/2}$	
						n = 0.2	n = 1.2	n = 0.2	n = 1.2
0.0	0.1	0.05	−0.1	0.1	0.2	0.419247	0.609219	0.950837	0.943978
0.35						0.440975	0.677945	0.850717	0.837593
0.7						0.455728	0.730783	0.760015	0.740866
1.05						0.466739	0.774059	0.675154	0.650189
1.40						0.475447	0.810908	0.594359	0.563754
0.2	0.0					0.430161	0.642566	0.906774	0.897148
	0.15					0.434151	0.655247	0.883660	0.872742
	0.3					0.438048	0.667966	0.853578	0.841209
	0.45					0.441849	0.680698	0.816654	0.802670
	0.6					0.445550	0.693419	0.773002	0.757236
		0.0				0.426576	0.631517	0.885735	0.875588
		0.05				0.432831	0.651015	0.892145	0.881675
		0.1				0.438590	0.669697	0.898032	0.887274
		0.15				0.443915	0.687628	0.903458	0.892441
		0.2				0.448858	0.704870	0.908476	0.897227
			0.01			0.430076	0.642924	0.712589	0.700499
			0.03			0.429638	0.641661	0.680967	0.668663
			0.05			0.429237	0.640514	0.650921	0.638481
			0.07			0.428905	0.639580	0.623853	0.611439
			0.09			0.428719	0.639098	0.602581	0.590570
			−0.1			0.432831	0.651015	0.892145	0.881675
			−0.3			0.438846	0.669475	1.186410	1.178900
			−0.5			0.445531	0.691096	1.416610	1.411230
			−0.7			0.452271	0.714027	1.590420	1.586380
			−0.9			0.458739	0.737141	1.722190	1.718990
				0.0		0.420499	0.612876	0.882485	0.872272
				0.25		0.443857	0.687907	0.901044	0.890361
				0.50		0.453964	0.724341	0.909434	0.898577
				0.75		0.459762	0.746487	0.914338	0.903392
				1.0		0.463593	0.761647	0.917602	0.906601
					0.0	0.432114	0.648635	0.957614	0.950436
					0.25	0.433008	0.651605	0.875818	0.864526
					0.5	0.433883	0.654530	0.794418	0.779016
					0.75	0.434740	0.657411	0.713403	0.693893
					1.0	0.435580	0.660250	0.632761	0.609148

6 Conclusion

This study analyses the time-dependent flow of two-phase magnetoelectric Carreau nanofluid with gyrostatic motile bacteria *via* a permeable oblique wedge with a heat source (sink), thermal radiation, and yield stress effects. The model simulation results led to these conclusions:

- Magnetization raises nanofluid speed and temperature, decreases BoLy concentration, and reverses by leaving the wedge surface. Also, the accretion magnetized parameter lowers the microbial field.
- The range of dilatant nanofluids is very close to that of pseudoplastic nanofluids in the case of the field of microorganisms.
- Increased electric parameter improves nanofluid velocity and temperature but decreases BoLy concentration. As the electric parameter drops, relative stability prevents concentration variation.
- Increased Eckert number raises the nanofluid temperature and decreases concentration and wedge surface distance.
- In suction, mass fluxing enhances nanofluid velocity and decreases temperatures, concentration, and microorganisms, while this is opposite for injection.

Table 3: Values $\mathrm{Sh}_x \mathrm{Re}_x^{-1/2}\left(\frac{2}{m+1}\right)^{1/2}$ and $\mathrm{Nh}_x \mathrm{Re}_x^{-1/2}\left(\frac{2}{m+1}\right)^{1/2}$ for different values of M, E, Ω, f_w, Nb, and Ec

M	E	Ω	f_w	Nb	Ec	$\mathrm{Sh}_x\mathrm{Re}_x^{-1/2}\left(\frac{2}{m+1}\right)^{1/2}$		$\mathrm{Nh}_x\mathrm{Re}_x^{-1/2}\left(\frac{2}{m+1}\right)^{1/2}$	
						n = 0.2	n = 1.2	n = 0.2	n = 1.2
0.00	0.1	0.05	−0.1	0.1	0.2	0.750661	0.745246	0.140706	0.136439
0.35						0.671618	0.661257	0.201782	0.199869
0.70						0.600012	0.584894	0.254787	0.255314
1.05						0.533016	0.513307	0.302923	0.305904
1.40						0.469231	0.445069	0.347765	0.353188
0.2	0.00					0.715874	0.708275	0.167570	0.164397
	0.15					0.697626	0.689007	0.182087	0.179277
	0.30					0.673877	0.664112	0.199806	0.197434
	0.45					0.644727	0.633687	0.220661	0.218812
	0.60					0.610265	0.597818	0.244592	0.243348
		0.00				0.699265	0.691254	0.174137	0.171451
		0.05				0.704325	0.696060	0.176889	0.173950
		0.10				0.708973	0.700479	0.179548	0.176361
		0.15				0.713257	0.704559	0.182117	0.178685
		0.20				0.717218	0.708337	0.184597	0.180934
			0.01			0.562571	0.553026	0.251507	0.249291
			0.03			0.537606	0.527891	0.285905	0.284111
			0.05			0.513885	0.504064	0.339571	0.338782
			0.07			0.492516	0.482715	0.429803	0.431628
			0.09			0.475722	0.466240	0.595889	0.605013
			−0.3			0.936636	0.930713	0.154563	0.150225
			−0.5			1.118380	1.114130	0.186483	0.181058
			−0.7			1.255600	1.252400	0.256571	0.250526
			−0.9			1.359620	1.357100	0.354800	0.348468
				0.075		0.939064	0.928046	0.0430169	0.0415501
				0.100		0.704325	0.696060	0.176889	0.173950
				0.125		0.563473	0.556860	0.257236	0.253410
				0.150		0.469568	0.464056	0.310809	0.306392
					0.00	0.756011	0.750344	0.145368	0.140886
					0.25	0.691435	0.682520	0.184750	0.182195
					0.50	0.627172	0.615012	0.223938	0.223306
					0.75	0.563213	0.547811	0.262938	0.264227
					1.00	0.499548	0.480906	0.301753	0.304966

- Increased Biot number due to BoLy thermal convection or convective boundary restrictions raise nanofluid temperatures, concentration, and microorganism outline.
- Increased yield stress results in increased velocity outlines away from the BoLy, improving nanofluid flow during shear thinning and thickening.
- For both dilatant and pseudoplastic nanofluids, increasing the exponent parameter increases flow velocity, especially away from the wedge BoLy in the center layers.
- Thermophoresis Nt increases nanofluid temperature profiles and concentration outlines, while it decreases them toward the border layer.
- The surface frictional force is increased by M, E, Ω, m, and Ec, whereas f_w decreases it. Ω, f_w, and m increase heat transference rates, whereas M, E, and Ec decrease them.
- All the mentioned parameters increase microorganisms' density in the nanofluid, but only the yield stress parameter increases mass transference.

In the future, the scope of the study can be expanded to include studying the effect of different secondary materials such as copper oxide, titanium oxide, *etc*., in terms of type and geometric shape and studying the thermal and hydrodynamic properties. It is also possible to explore the

effect of irregular magnetic and electric fields on the stability of this flow. It is also possible to examine the chemical diffusion and biological interactions to understand the extent of the response of these microorganisms. In addition, it can also be used to study the effect of changing boundary conditions such as oscillating boundaries and analyze the stability of the thermodynamics of the system.

Acknowledgments: The authors extend their appreciation to the Deanship of Scientific Research at Northern Border University, Arar, KSA for funding this research work through the project number NBU-FFR-2025-3021-02. The authors are thankful to the Deanship of Graduate Studies and Scientific Research at University of Bisha for supporting this work through the Fast-Track Research Support Program.

Funding information: This work was funded by the Deanship of Scientific Research at Northern Border University, Arar, KSA through the project number NBU-FFR-2025-3021-02.

Author contributions: Conceptualization: E.M.E. and M.A.; data curation: M.A., M.R.E., and A.S.A.; formal analysis: E.M.E., M.A., and M.R.E.; investigation: E.M.E., M.A., and M.R.E.; methodology: M.A. and A.S.A.; project administration: E.M.E. and M.R.E.; software: E.M.E. and M.A.; supervision: M.A. and M.R.E.; validation: M.A. and A.S.A.; visualization: M.A.; writing – original draft: E.M.E., M.A., A.S.A., and M.R.E.; writing – review and editing: E.M.E. and M.R.E. All authors have accepted responsibility for the entire content of this manuscript and approved its submission.

Conflict of interest: The authors state no conflict of interest.

Data availability statement: All data generated or analyzed during this study are included in this published article.

References

[1] Schowalter WR. The application of boundary-layer theory to power-law pseudoplastic fluids: Similar solutions. AIChE J. 1960;6(1):24–8.
[2] Acrivos A, Shah M, Petersen E. Momentum and heat transfer in laminar boundary-layer flows of non-Newtonian fluids past external surfaces. AIChE J. 1960;6(2):312–7.
[3] Acrivos A. A theoretical analysis of laminar natural convection heat transfer to non-Newtonian fluids. AIChE J. 1960;6(4):584–90.
[4] Fox V, Erickson L, Fan L. The laminar boundary layer on a moving continuous flat sheet immersed in a non-Newtonian fluid. AIChE J. 1969;15(3):327–33.
[5] Bird RB, Armstrong RC, Hassager O. Dynamics of polymeric liquids. Fluid mechanics. New York: Wiley; Vol. 1, 1987.
[6] Carreau PJ. Rheological equations from molecular network theories. Trans Soc Rheol. 1972;16(1):99–127.
[7] Šiška B, Bendová H, Machač I. Terminal velocity of non-spherical particles falling through a Carreau model liquid. Chem Eng Process: Process Intensif. 2005;44(12):1312–9.
[8] Hyun YH, Lim ST, Choi HJ, Jhon MS. Rheology of poly (ethylene oxide)/organoclay nanocomposites. Macromolecules. 2001;34(23):8084–93.
[9] Bush M, Phan-Thien N. Drag force on a sphere in creeping motion through a Carreau model fluid. J Non-Newtonian Fluid Mech. 1984;16(3):303–13.
[10] Chhabra R, Uhlherr P. Creeping motion of spheres through shear-thinning elastic fluids described by the Carreau viscosity equation. Rheol Acta. 1980;19:187–95.
[11] Hsu J, Yeh S. Drag on two coaxial rigid spheres moving along the axis of a cylinder filled with Carreau fluid. Powder Technol. 2008;182(1):56–71.
[12] Uddin J, Marston JO, Thoroddsen ST. Squeeze flow of a Carreau fluid during sphere impact. Phys Fluids. 2012;24(7):073104.
[13] Tshehla M. The flow of a Carreau fluid down an incline with a free surface. Int J Phys Sci. 2011;6(16):3896–3910.
[14] Olajuwon IB. Convection heat and mass transfer in a hydromagnetic Carreau fluid past a vertical porous plate in presence of thermal radiation and thermal diffusion. Therm Sci. 2011;15(suppl. 2):241–52.
[15] Griffiths PT. Flow of a generalised Newtonian fluid due to a rotating disk. J Non-Newtonian Fluid Mech. 2015;221:9–17.
[16] Sakiadis BC. Boundary-layer behavior on continuous solid surfaces: I. Boundary-layer equations for two-dimensional and axisymmetric flow. AIChE J. 1961;7(1):26–8.
[17] Crane LJ. Flow past a stretching plate, Zeitschrift für angewandte Mathematik und Physik. ZAMP. 1970;21:645–7.
[18] Cortell R. Viscous flow and heat transfer over a nonlinearly stretching sheet. Appl Math Comput. 2007;184(2):864–73.
[19] Andersson H, Kumaran V. On sheet-driven motion of power-law fluids. Int J Non-Linear Mech. 2006;41(10):1228–34.
[20] Chamkha AJ, Al-Humoud JM. Mixed convection heat and mass transfer of non-Newtonian fluids from a permeable surface embedded in a porous medium. Int J Numer Methods Heat Fluid Flow. 2007;17(2):195–212.
[21] Hady F, Ibrahim F, Abdel-Gaied S, Eid M. Boundary-layer non-Newtonian flow over vertical plate in porous medium saturated with nanofluid. Appl Math Mech. 2011;32:1577–86.
[22] Kishan N, Reddy BS. MHD effects on non-Newtonian power-law fluid past a continuously moving porous flat plate with heat flux and viscous dissipation. Int J Appl Mech Eng. 2013;18(2):425–45.
[23] Mahmoud MA. Chemical reaction and variable viscosity effects on flow and mass transfer of a non-Newtonian visco-elastic fluid past a stretching surface embedded in a porous medium. Meccanica. 2010;45:835–46.
[24] Alfvén H. Existence of electromagnetic-hydrodynamic waves. Nature. 1942;150(3805):405–6.
[25] Pavlov K. Magnetohydrodynamic flow of an incompressible viscous fluid caused by deformation of a plane surface. Magnitnaya Gidrodinamika. 1974;4(1):146–7.

[26] Waqas H, Khan SU, Imran M, Bhatti M. Thermally developed Falkner–Skan bioconvection flow of a magnetized nanofluid in the presence of a motile gyrotactic microorganism: Buongiorno's nanofluid model. Phys Scr. 2019;94(11):115304.
[27] Waqas H, Khan SU, Bhatti M, Imran M. Significance of bioconvection in chemical reactive flow of magnetized Carreau–Yasuda nanofluid with thermal radiation and second-order slip. J Therm Anal Calorim. 2020;140(3):1293–306.
[28] Waqas H, Imran M, Muhammad T, Sait SM, Ellahi R. Numerical investigation on bioconvection flow of Oldroyd-B nanofluid with nonlinear thermal radiation and motile microorganisms over rotating disk. J Therm Anal Calorim. 2021;145:523–39.
[29] Muhammad T, Alamri SZ, Waqas H, Habib D, Ellahi R. Bioconvection flow of magnetized Carreau nanofluid under the influence of slip over a wedge with motile microorganisms. J Therm Anal Calorim. 2021;143:945–57.
[30] Khan M, Ali W, Ahmed J. A hybrid approach to study the influence of Hall current in radiative nanofluid flow over a rotating disk. Appl Nanosci. 2020;10(12):5167–77.
[31] Mahanthesh B, Gireesha B, Shehzad SA, Ibrar N, Thriveni K. Analysis of a magnetic field and Hall effects in nanoliquid flow under insertion of dust particles. Heat Transf. 2020;49(3):1632–48.
[32] Khan W, Makinde O, Khan Z. MHD boundary layer flow of a nanofluid containing gyrotactic microorganisms past a vertical plate with Navier slip. Int J Heat Mass Transf. 2014;74:285–91.
[33] Chakraborty T, Das K, Kundu PK. Framing the impact of external magnetic field on bioconvection of a nanofluid flow containing gyrotactic microorganisms with convective boundary conditions. Alex Eng J. 2018;57(1):61–71.
[34] Waqas H, Khan SU, Hassan M, Bhatti M, Imran M. Analysis on the bioconvection flow of modified second-grade nanofluid containing gyrotactic microorganisms and nanoparticles. J Mol Liq. 2019;291:111231.
[35] Patil P, Goudar B, Patil M, Momoniat E. Bioconvective periodic MHD Eyring-Powell fluid flow around a rotating cone: influence of multiple diffusions and oxytactic microorganisms. Alex Eng J. 2023;81:636–55.
[36] Patil P, Goudar B, Momoniat E. Magnetized bioconvective micropolar nanofluid flow over a wedge in the presence of oxytactic microorganisms. Case Stud Therm Eng. 2023;49:103284.
[37] Patil P, Goudar B, Patil M, Momoniat E. Unsteady magneto bioconvective Sutterby nanofluid flow: influence of g-Jitter effect. Chin J Phys. 2024;89:565–81.
[38] Hussanan A, Salleh MZ, Khan I, Shafie S. Convection heat transfer in micropolar nanofluids with oxide nanoparticles in water, kerosene and engine oil. J Mol Liq. 2017;229:482–8.
[39] Hussanan A, Salleh MZ, Alkasasbeh HT, Khan I. MHD flow and heat transfer in a Casson fluid over a nonlinearly stretching sheet with Newtonian heating. Heat Transf Res. 2018;49(12):1185–98.
[40] Eid MR. 3-D flow of magnetic rotating hybridizing nanoliquid in parabolic trough solar collector: Implementing Cattaneo-Christov heat flux theory and Centripetal and Coriolis forces. Mathematics. 2022;10(15):2605.
[41] Sangeetha E, De P. Stagnation point flow of bioconvective MHD nanofluids over Darcy Forchheimer porous medium with thermal radiation and buoyancy effect. BioNanoScience. 2023;13(3):1022–35.
[42] Sangeetha E, De P. Bioconvective Casson nanofluid flow toward stagnation point in non-Darcy porous medium with buoyancy effects, chemical reaction, and thermal radiation. Heat Transf. 2023;52(2):1529–51.
[43] Sangeetha E, De P, Das R. Hall and ion effects on bioconvective Maxwell nanofluid in non-darcy porous medium. Spec Top Rev Porous Media: An Int J. 2023;14(4):1–30.
[44] Al Qarni A, Elsaid EM, Abdel-Aty A-H, Eid MR. Heat transfer efficacy and flow progress of tripartite diffusion in magneto-radiative Reiner-Philippoff nanofluid in porous Darcy-Forchheimer substance with heat source. Case Stud Therm Eng. 2023;45:103022.
[45] Rajeswari PM, De P. Multi-stratified effects on stagnation point nanofluid flow with gyrotactic microorganisms over porous medium. J Porous Media. 2024;27(5):67–84.
[46] Khan M, Azam M, Alshomrani A. Unsteady slip flow of Carreau nanofluid over a wedge with nonlinear radiation and new mass flux condition. Results Phys. 2017;7:2261–70.
[47] Gangadhar K, Sarma SVK, Chamkha AJ. Rheological behaviour of Carreau liquid past a wedge surface with binary chemical reaction. Proceedings of the Institution of Mechanical Engineers, Part E: Journal of Process Mechanical Engineering; 2023. p. 09544089231207412. doi: 10.1177/09544089231207412.
[48] Patil P, Goudar B. Entropy analysis in a mixed convective Carreau nanofluid flow around a wedge: impact of activation energy and sinusoidal magnetic field. J Taibah Univ Sci. 2024;18(1):2329373.
[49] Patil P, Kulkarni M, Tonannavar J. A computational study of the triple-diffusive nonlinear convective nanoliquid flow over a wedge under convective boundary constraints. Int Commun Heat Mass Transf. 2021;128:105561.
[50] Patil P, Shankar H. A comprehensive investigation of combined convective nanoliquid flow past a wedge using a local thermal non-equilibrium model. Eur Phys J Plus. 2023;138(1):1–17.